CHAPTER 4

From Polymeric to Nanostructured Carbon Nitride Thin Films: A Study of Electrode Distance

4 FROM POLYMERIC TO NANOSTRUCTURED CARBON NITRIDE THIN FILMS: A STUDY OF ELECTRODE DISTANCE

4.1 Introduction and Overview

This chapter presents the fabrication, characterization and discussion of hydrogenated carbon nitride thin films (CN$_x$:H) deposited as a function of electrode distance. The significant differences in structure with the changes in electrode distance are highlighted. It is a prelude to Chapter 5 which presents the study on the polymeric carbon nitride and the subsequent Chapter 6 which details the study on nanostructured carbon nitride thin films.

The main focus of this chapter is to introduce the two different structures obtained through the manipulation of the electrode distance of the home-built rf PECVD which employs a parallel-plate electrode configuration. The structural evolution was studied by means of field emission scanning electron spectroscopy (FESEM), Auger electron spectroscopy (AES), Fourier transform infrared spectroscopy (FTIR) and Raman scattering. Additionally, optical characterizations of films deposited on quartz and photoluminescence for films on Si substrates are also presented. The FESEM analysis was carried out to investigate the structural and morphological properties, while AES, FTIR and Raman were done to study the chemical bonding, structure and composition of the materials.

4.2   Deposition Parameters

In this chapter, the effects of varying the parallel-plate electrode distance D_E, were studied. Six sets of films were deposited on quartz slides and polished p-type (111) silicon substrates for D_E fixed at 6 to 1 cm, which was varied in increments of 1 cm. Other deposition parameters were kept constant and are summarized in Table 4.1 below. Due to the increase in ion bombardment, the substrate temperature increases gradually during the deposition process from the initial 100°C fixed prior to the deposition. However after an hour through the deposition, the temperature begins to saturate. The variation of the substrate temperature as a function of deposition time has been shown in Figure 3.3 of Chapter 3. The value of the final temperature increase as D_E decreases.

Table 4.1: Deposition parameters for the study of the effects of electrode distance on the structural properties of CN$_x$:H thin films.

	Parameter	Set values
1.	Electrode distance *	6 to 1 cm
2.	rf power	80W (1.02 W/cm^2)
3.	Initial substrate temperature	100°C
4.	Chamber base pressure	~1×10^{-5} mbar
5.	Methane (CH$_4$) mass flow-rate	20 sccm
6.	Nitrogen (N$_2$) mass flow-rate	47 sccm
7.	[N$_2$/(N$_2$+CH$_4$)]	0.70
8.	Deposition time	90 minutes
9.	Deposition pressure	0.8 mbar

*indicates the variable parameter for the study

4.3 Experimental Results

4.3.1 Field emission scanning electron microscopy (FESEM)

The variation of surface and cross-sectional image as a function of electrode distance D_E is shown in Figure 4.1.

	Surface images		Cross-sectional images	
	Low magnification	High magnification	Low magnification	High magnification
6 cm				
5 cm				
4 cm				
3 cm				
2 cm				
1 cm				
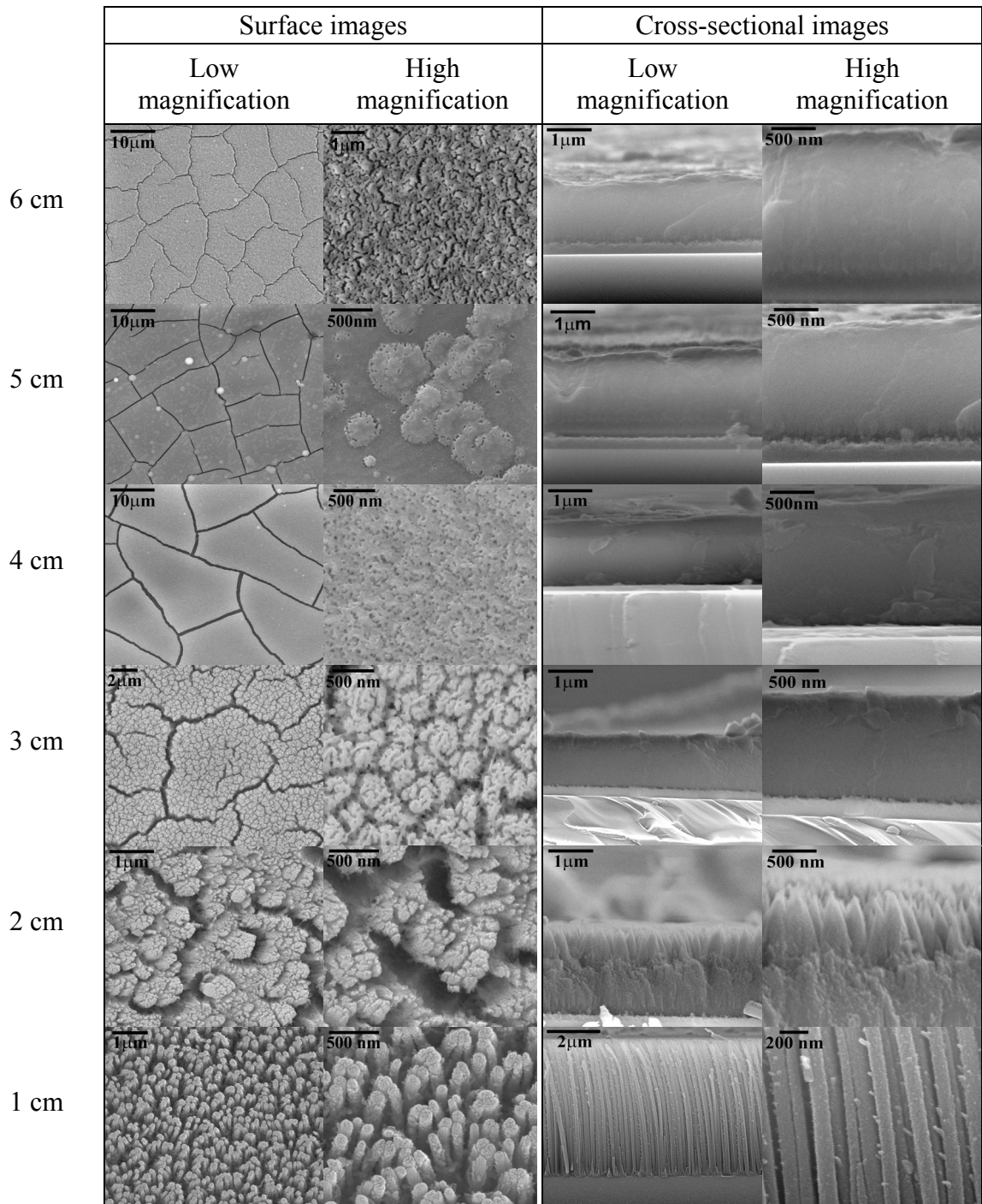
Figure 4.1: Variation of FESEM surface and cross-sectional images spectra for films deposited as a function of electrode distance.

For clarification the FESEM surface and cross-sectional images for D_E of 6, 3, 2 and 1 cm are shown in Figure 4.2 and 4.3, respectively.
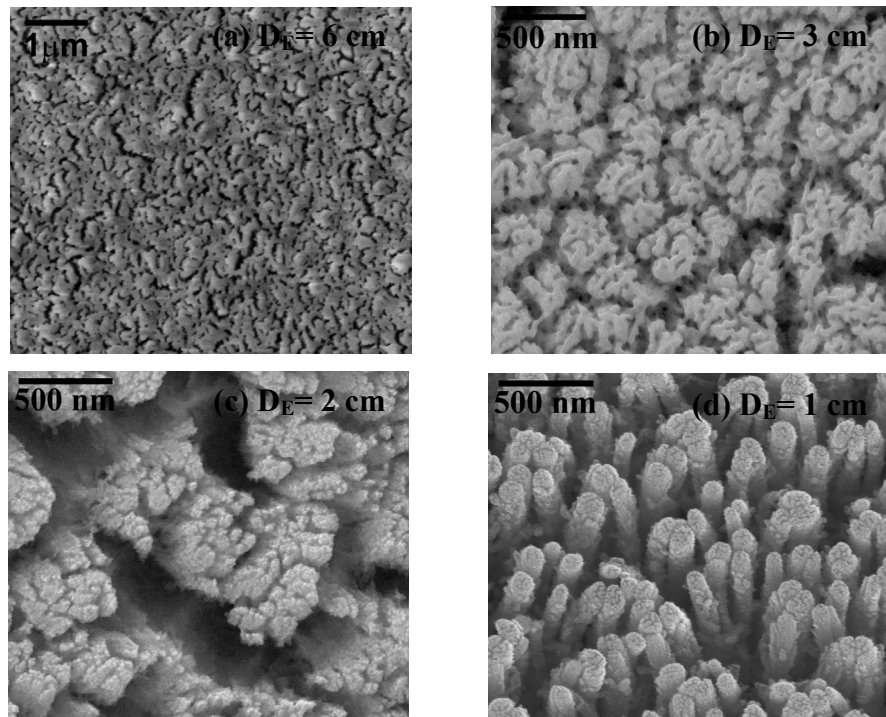
Figure 4.2: Variation of FESEM surface images for films deposited at electrode distance of (a) 6 cm, (b) 3 cm, (c) 2 cm and (d) 1 cm.
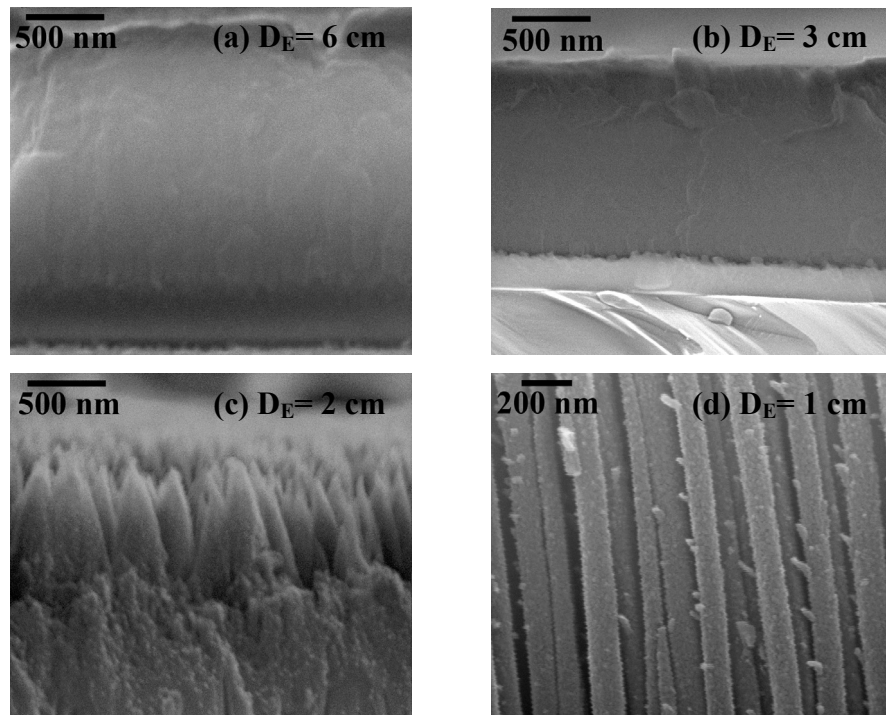
Figure 4.3: Variation of FESEM cross-sectional images for films deposited at electrode distance of 6, 3, 2 and 1 cm.

Within D$_E$ range of 6 to 3 cm the structure of the thin films are similar with the formation of quite a uniform amorphous thin film. By further decreasing D$_E$, a more drastic structural change is observed beginning with the film deposited at D$_E$ of 2 cm. From the cross-sectional image seen in Figure 4.3(c), this film is made up of aligned spear-like submicron structures which protrude out from what appears to be an amorphous layer. It is well worth noting that the surface image of the film deposited at D$_E$ of 3 cm also shows a similar profile to that of the sample prepared at 2 cm, but the extent of the structural similarity is limited to the film sub-surface as is evident from the cross-sectional image. Subsequent lowering of D$_E$ to 1 cm results in the formation of highly vertically aligned nanostructures apparent both from the surface and cross-sectional images.

The variation in growth rate measured directly from the FESEM cross-sectional images is shown in Figure 4.4.
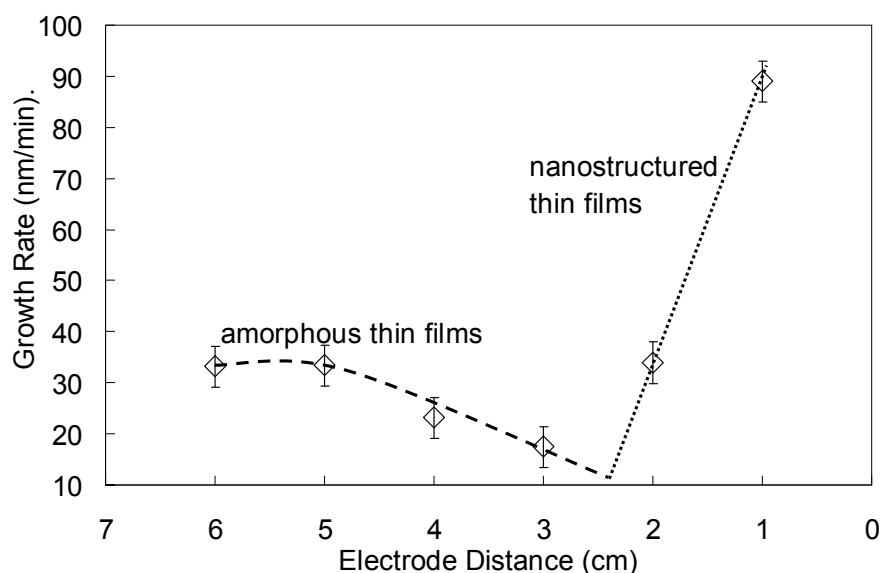
Figure 4.4: Variation in growth rate for the thin films and nanostructures calculated from the FESEM cross-sectional images, spectra for films deposited as a function of electrode distance. Lines are as guide to the eyes.

The growth rate is calculated using the thickness of the polymeric films and length of the nanostructures, measured perpendicular to the surface of the substrates. Averages of 50 measurement points along the width of the film were taken where calculation errors were calculated from standard deviation. The growth rate decreases significantly in the D_E range of 6 to 3 cm followed by a sharp increase in the growth rate of the nanostructures as D_E is further reduced from 2 to 1 cm.

The growth rate remains almost the same for D_E of 5 and 6 cm and is due to the formation of dust for D_E of 6 cm, which does not contribute significantly to the thickness of the film. Furthermore these dust particles were removed from the film in a flow of nitrogen right after the deposition. The decrease in growth rate within the D_E range of 6 − 3 cm, is attributed to ion bombardment on the growing surface. The increase in ion bombardment is attributed to the increase in the electric field between the electrodes as D_E decreases. However, within this distance the structures of these films remain the same. By further reducing the electrode distance below the critical D_E of 2 cm, the increase in bombardment results in a suppression of the growth of the amorphous component relative to those of the nanostructures (including both the spear-like and nanorods). These nanostructures are expected to be harder that the amorphous component and thus are harder to etch out. As a result, the formation of the nanostructured films is preferred. Similar to those seen for nanotips produced in CH$_4$/N$_2$/H$_2$ plasma by planar microwave PECVD at low temperature (Chih et al. 2006), these nanostructures do not require any metal catalyst to grow and instead are seen to be able to grow directly on the Si substrate.

To study the importance of nitrogen in the formation of these nanostructures, three additional samples were deposited under the same deposition conditions but from

a pure CH$_4$ plasma and the mixtures of CH$_4$ and hydrogen or argon. The surface images

of the films obtained from these depositions are depicted in Figure 4.5
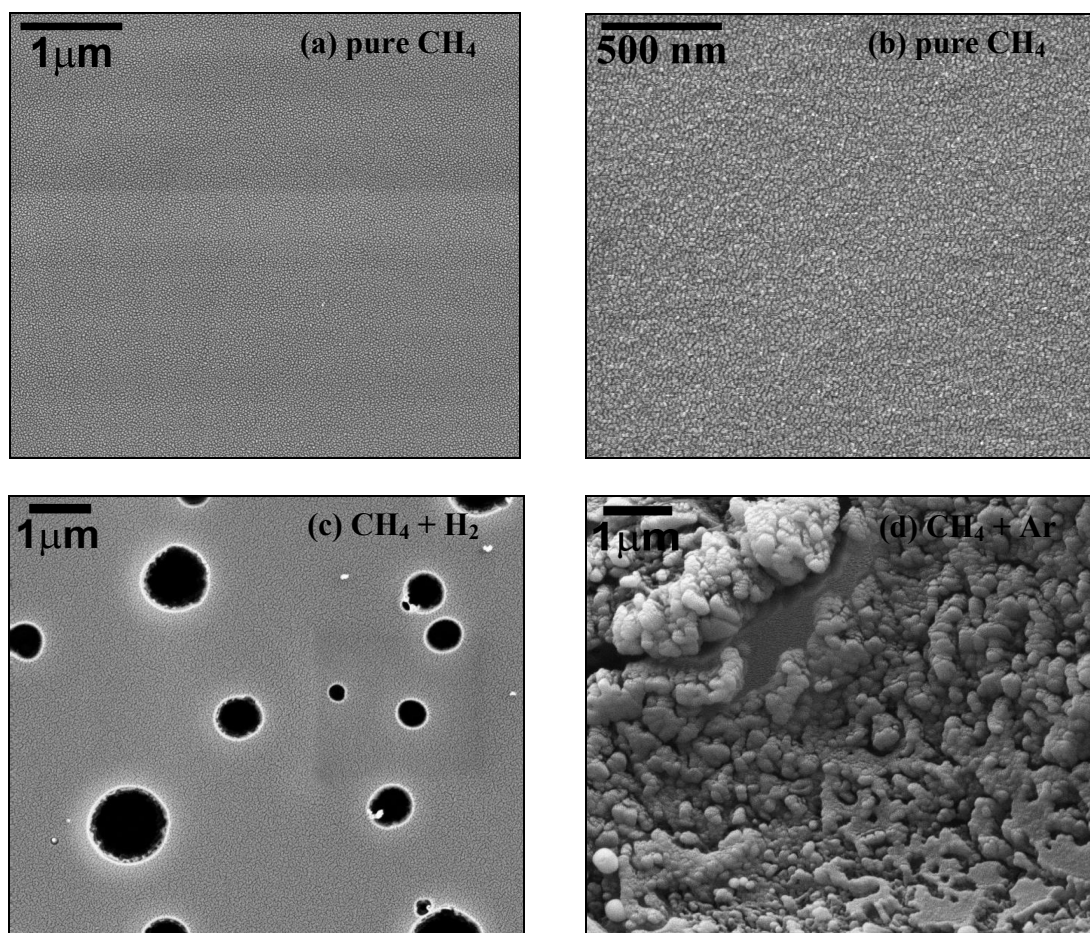
Figure 4.5: FESEM surface image of films grown on silicon substrate from pure CH$_4$ (a)

and (b), mixture of CH$_4$ and H$_2$ (c) and mixture of CH$_4$ and Ar (d) gases.

Image (b) is the higher magnification image of (a) shown for clarification.

The images clearly show that nanostructures were not formed although each

deposition forms very unique films. The deposition from pure CH$_4$ forms film with a

smooth uniform surface. The deposition from a mixture of CH$_4$ and H$_2$ also forms a

smooth uniform surface but with random size crater-like structures scattered throughout

the film surface. These may be the result of selective hydrogen etching occurring in

regions with weak bonds on the surface. On the other hand, the mixture of CH$_4$ and Ar results in a film with grainy-like features scattered within irregular shaped fragmented masses. This morphology may be the result of high ion bombardments on the surface by the heavier argon ions. In the process of film formation the surface is also sputtered by the Ar ions thus forming these irregular features.

Thus, it was observed that the nitrogen incorporation is crucial in the formation of these nanostructures. High Ar ion bombardment on the growth surface and structural modification as a result of H etching effects are shown to be ineffective in forming such nanostructures. The role of N atoms in the formation of nanostructures is expected to be either as a substitutional element in the carbon network, reactive species in the plasma reactions and/or as bombarding element on the growing surface. With this in mind a series of measurements were carried out to determine the nitrogen content and bonding in these films. The purpose of this is to give a clearer picture into the effect and contribution of the nitrogen incorporation.

4.3.2   *Auger electron spectroscopy*

The AES analysis was carried out to determine the relative composition of C and N in the material. The AES spectra as a function of D$_E$ are shown in Figure 4.6, where the carbon and nitrogen content were calculated from their corresponding peaks. The variation of the nitrogen to carbon, N/C ratio is shown in Figure 4.7. From these results, it is seen that the incorporation of nitrogen, although it varies, is effectively preserved in the material regardless of D$_E$ and changes in structure.
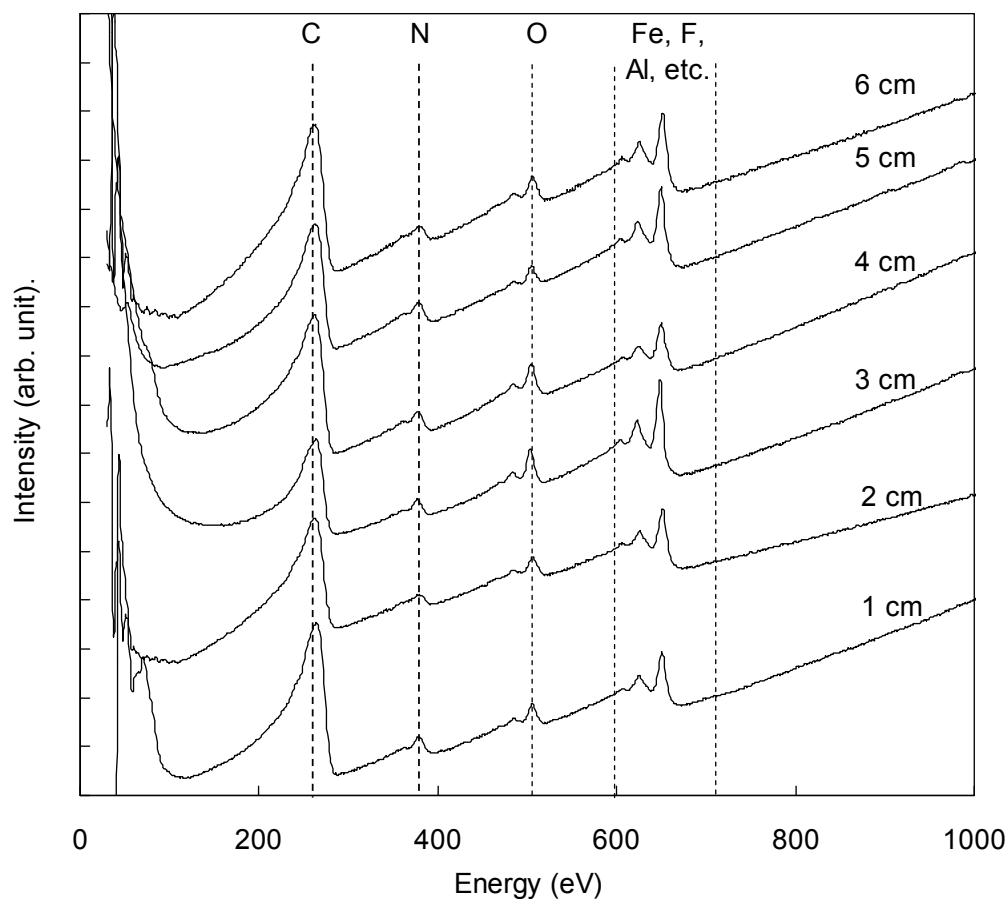
Figure 4.6: Variation in AES spectra for films deposited

as function of electrode distance.

The variation in N/C appears to mirror the thickness variation in which two distinct regions corresponding to different trends in the changes in N/C is observed. These regions could be separated out into the D_E range of 6 to 3 cm corresponding to the formation of polymeric a-CN$_x$:H films and to D_E range of 3 to 1 cm where the nanostructured films were obtained. Within the region pertaining to the formation of the polymeric films, a slight increase in N incorporation is seen for films deposited at D_E of 5 cm. Interestingly, the N/C ratio at D_E of 6 cm is lower than that of the films grown at 5 cm which may be due to formation of dust on the film at 6 cm. It is predicted that the dust consist of a-CN$_x$:H particles in which N may be more inclined to be incorporated. With the removal of the dust prior to any measurement carried on these films, the N/C ratio effectively decreases for the remaining film.
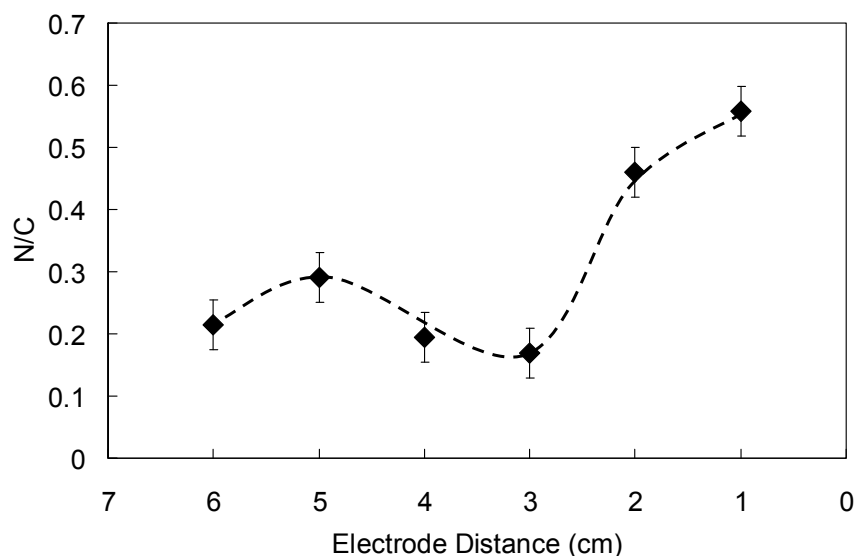
Figure 4.7: Variation of nitrogen to carbon N/C ratio spectra for films deposited

as a function of electrode distance.

However the most significant aspect in this AES result is seen in the increase in N incorporation with the formation of the nanostructured films, and in particular the vertically aligned nanostructured film obtained at D_E of 1 cm. At D_E of 1 cm, the value of N/C is the highest at (0.56 ± 0.01) which corresponded to a N content of (36 ± 1) atm%. This shows that not only does N incorporation need to be relatively high for the formation of these nanostructures but the reverse is also true whereby to obtain carbon nitride films with high N incorporation it may be necessary to prepare the films in a nanostructured form.

4.3.3   Raman scattering

The Raman spectra as a function of D_E are shown in Figure 4.8. Figure 4.8 (a) shows the raw Raman spectra where the spectra are dominated by a strong photoluminescence (PL) background. This results in a slope in the baseline.

Interestingly, the baseline gives a negative slope, a trend normally seen for higher excitation energy (McMillan et al. 2009) compared to that of visible Raman. This could be related to the difference in PL spectra of the films in this work to those reported elsewhere. The presence of a high PL background is an indication of high hydrogen content in the film and the profile of such spectra is normally seen for polymeric-like films (Chu and Li 2006; Wang et al. 2006b). Thus the high PL background and spectra profile, particularly for D_E of 4 cm and 5 cm, supports that the films produced with D_E of 6-3 cm are polymeric. With a decrease in D_E, a progressive decrease in the PL background is observed ending with an almost flat baseline for D_E of 1 cm which coincides with the changes in the structure.

For further analysis of the spectra, the PL background is eliminated using a non-linear fitting. The baseline is extracted from these spectra, giving the corrected spectra as shown in Figure 4.8 (b). Included are the Gaussian fittings of these spectra in which the D and G lines were determined. The absence of these peaks for D_E of 3 cm coincides with its position as the turning point of the structural transformation. Also, the low intensities of the peaks for D_E of 6 cm may be due to the formation of dust which may be amorphous in nature and is integrated into the surface of the films. A progressive change in the D and G lines intensities is observed with an increase in the relative intensity of the G band. From these fitting parameters, the band-position (ω) and bandwidth (FWHM) of both G and D bands, and the ratio of the integrated intensities of D band to G band, I_D/I_G were calculated. Figure 4.9 shows the variation in peak position for the G line (ω_G) and its width (FWHM$_G$), peak position for the D line (ω_D) and its width (FWHM$_D$), and I_D/I_G ratio of the deposited films as a function of electrode distance.
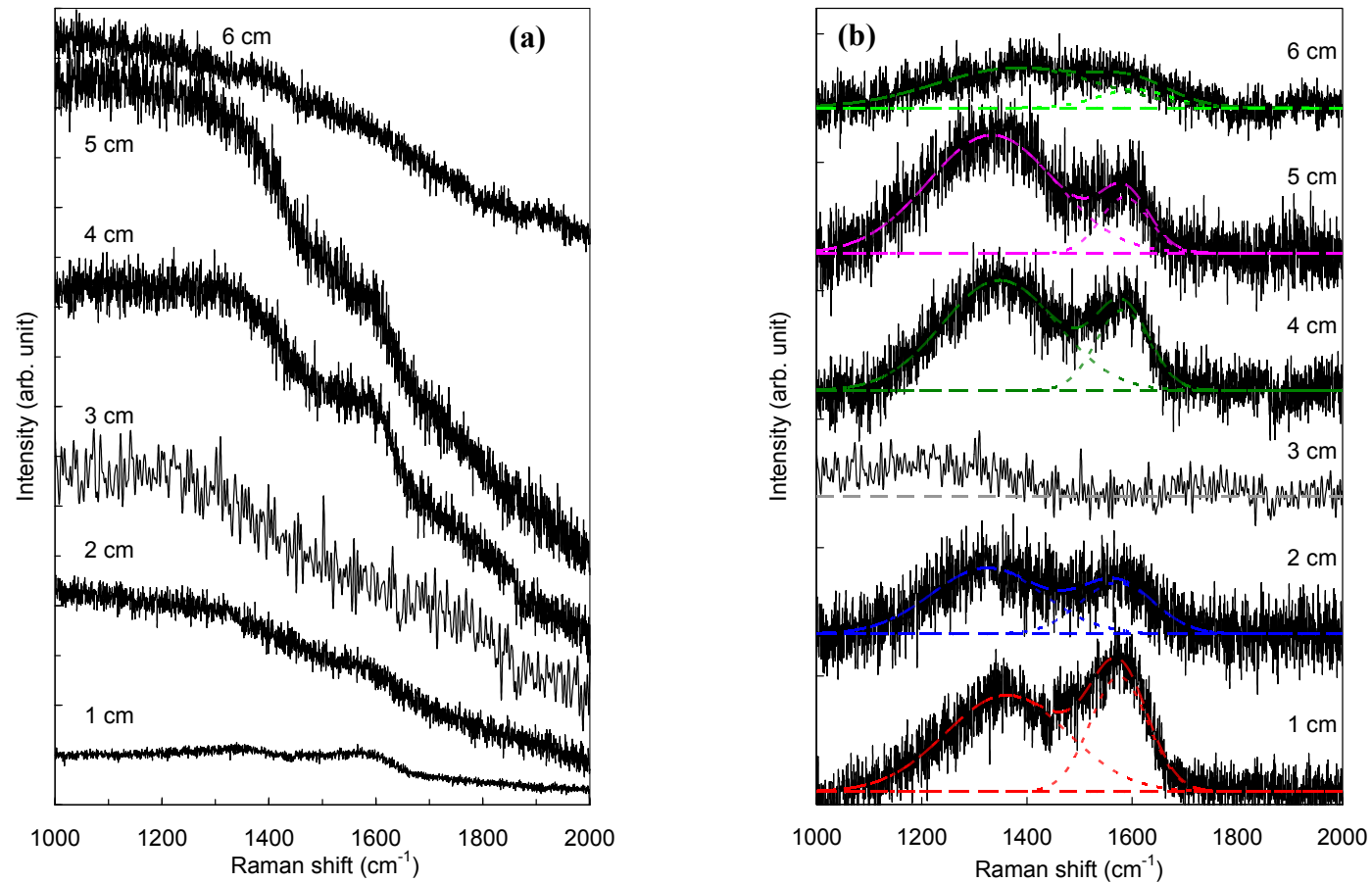
Figure 4.8: Variation in Raman scattering spectra for films deposited as a function of electrode distance, whereby (a) shows the raw data obtained with a significant decrease in photoluminescence background with decrease in electrode distance, and (b) shows the deconvolution of the Raman spectra after photoluminescence background extraction.
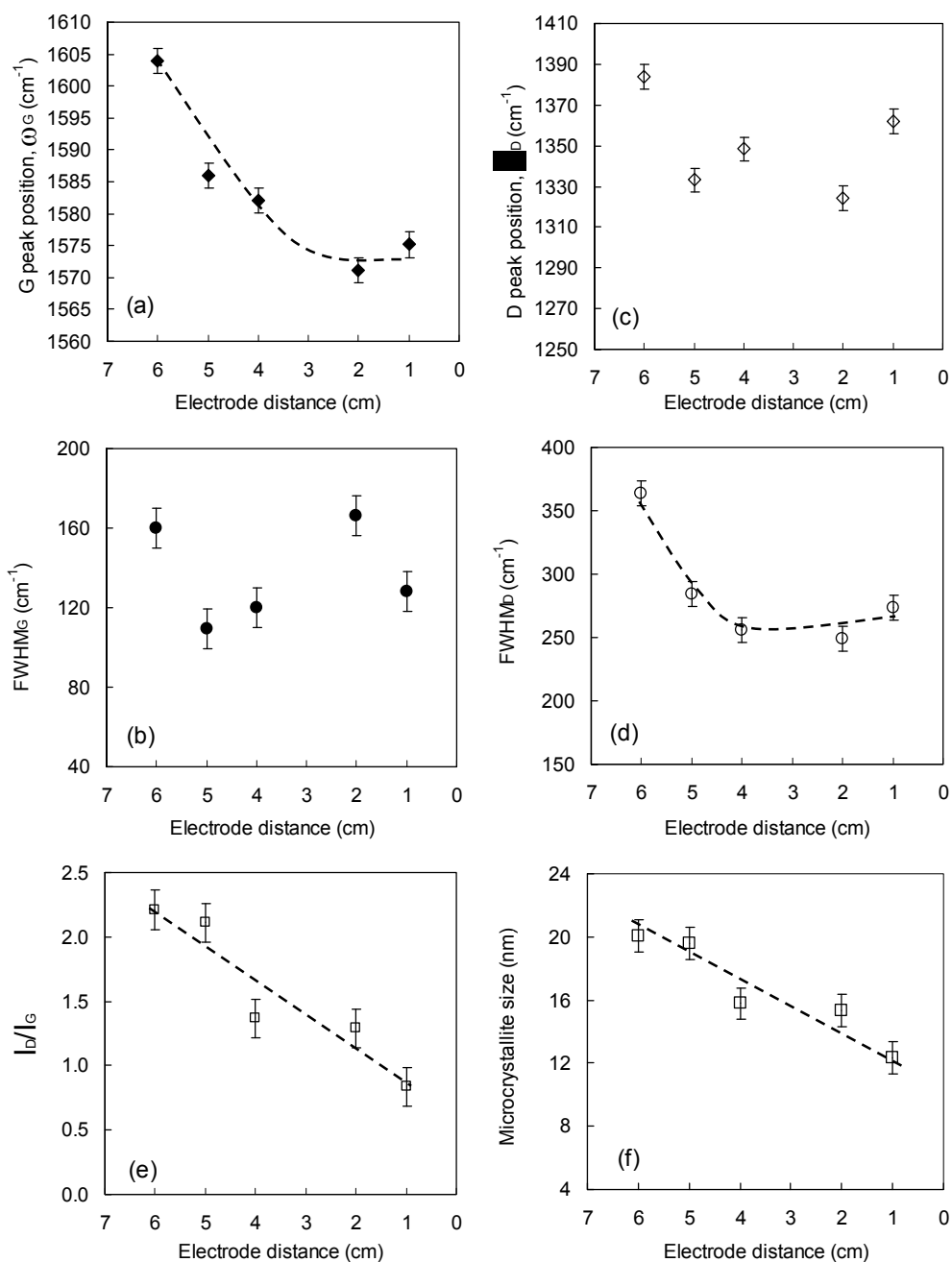
Figure 4.9: Gaussian fitting results for films deposited

as a function of electrode distance

In Figure 4.9 a trend is seen for the G band position, D bandwidth and the I$_D$/I$_G$ ratio and the corresponding variation in microcrystallite size. The G bandwidth and D peak position appear somewhat inconsistent and for simplicity is not included in the assessment of the Raman shift. In general, the G band position decreases with the

decrease in electrode distance, D_E, although its value remains almost the same for the formation for the nanostructures at D_E of 2 and 1 cm. Likewise the D bandwidth decreases and then saturates for D_E below 3 cm. This may be due to the similarity in surface morphologies even for D_E of 3 cm which appears akin to that of 2 cm which was seen from Figure 4.2. This is deduced from the fact that the Raman measurements were limited to the subsurface level and are very much dependent on the surface characteristics. However the I_D/I_G ratio shows a consistent trend that indicates a gradual change in the film structure.

In general, it can be seen from Figure 4.9 (e) the I_D/I_G ratio is larger than 1.1, which further supports the suggestion that these films belongs to the Stage 2 of the amorphization trajectories described previously. This ratio decreases with decrease in D_E. This indicates a decrease in the ordering in these films and is related to the decrease in number and/or size of the sp^2 clusters in the films. This is supported by the red-shift in the G peak position which reflects a larger degree of bond angle or bond length disorder. However it is noted that the G peak position for D_E between 6 to 3 cm is above that of graphitic carbon (1575 cm^{-1}) which shows that the characteristics of these films is governed by high graphene clustering. In particular, the G peak position for D_E of 6 cm at (1604 ± 1) cm^{-1} shows that these films are dominated by graphene-like ordered clusters.

Thus, on one hand, the increase in the G band position and the increase in the I_D/I_G ratio films with the increase in D_E (towards the formation of polymeric films) indicates an increase in sp^2 cluster size with predominantly graphene structures. While on the other hand, the red shift in the G band with the decrease in D_E (towards the formation of nanostructured films) indicates an increase in non six-fold rings in the sp^2-

clusters and/or a decrease in the graphitic cluster size. The former is supported by the increase in nitrogen incorporation in these films with the decrease in D_E determined from AES results. As discussed, sp^2-type incorporation of nitrogen would generate a significant amount of non six-fold atomic structures in the CN$_x$ films. However, it is seen from Figure 4.9(f) that the graphitic microcrystallite size decreases as D_E decreased. Also, the value of the G peak for films deposited at D_E of 2 and 1 cm, i.e. the nanostructured CN$_x$:H films, still remains close to that of graphitic films and indicates the dominance of sp^2 clusters consisting of six-fold ring configurations in its structure. Thus, this indicates that small graphitic clusters are of significance in the formation of the nanostructures, as compared to the graphene-like clustering in the polymeric films. Nevertheless, compared to the polymeric films the size and/or number of these six-fold ring clusters are significantly less, as indicated by the decrease in I_D/I_G ratio. Here, the results imply that the increase in non six-fold ring with the decrease in D_E, may cause the segregation and isolation of the graphitic six-fold rings into smaller clusters.

An opposite trend is seen in the reduction of the bandwidth of the D band with a decrease in D_E, as seen in Figure 4.9 (d). The decreasing trend indicates an increase in ordering which could be due to the removal of bond-angle disorder. However, this contradicts the decrease in G band position and I_D/I_G ratio which shows that the bond-angle and bond length disorder increases with decrease in D_E. Thus the decrease in the width of the D band may instead be due to an increase in the dominance of crystallites in the films with regards to the effects and distribution of these crystallites on the structure of the films. It should be remembered however, that the visible Raman is related closely to the changes in sp^2 bonds in the films and does not describe the changes which may occur for sp^1 and sp^3 bonds in the films. For that reason a detailed

study of the bonding properties is carried out by studying the infrared characteristics of the films.

4.3.4   Fourier transform infrared spectroscopy (FTIR)

The FTIR studies were carried out to obtain more information regarding the bonding configuration of the growing films as a function of D_E. These spectra were normalized by the film thickness which in most cases enables more comparative analysis to be done. However since the nanostructures would give a significantly different density which would influence the intensity of the absorption coefficient compared to the polymeric films, detailed comparative analysis were avoided. Nevertheless, this would not effect the peak position or the shape profile of the band and is still regarded as valid in the current study.

As shown in Figure 4.10 the spectra are similar in appearance and could be divided into 3 major regions. These include (i) the sp^2 phases comprising, among others, the C=C and/or C=N, and N-H bonds within the wavenumber range of 1300–1800 cm^{-1}, (ii) the sp^1 phase associated with the C≡N groups within the range of 1800–2200 cm^{-1}, and finally (iii) the groups correlated to the presence of hydrogen comprising of the sp^2 and sp^3 phases of C-H groups within the range of 2800–3000 cm^{-1} and the hydroxyl N-H and/or O-H groups within the range of 3000-3800 cm^{-1} (Motta and Pereyra 2004; Mutsukura and Akita, 2000). For clarification the individual stacked spectra for each region is shown in Figure 4.11.
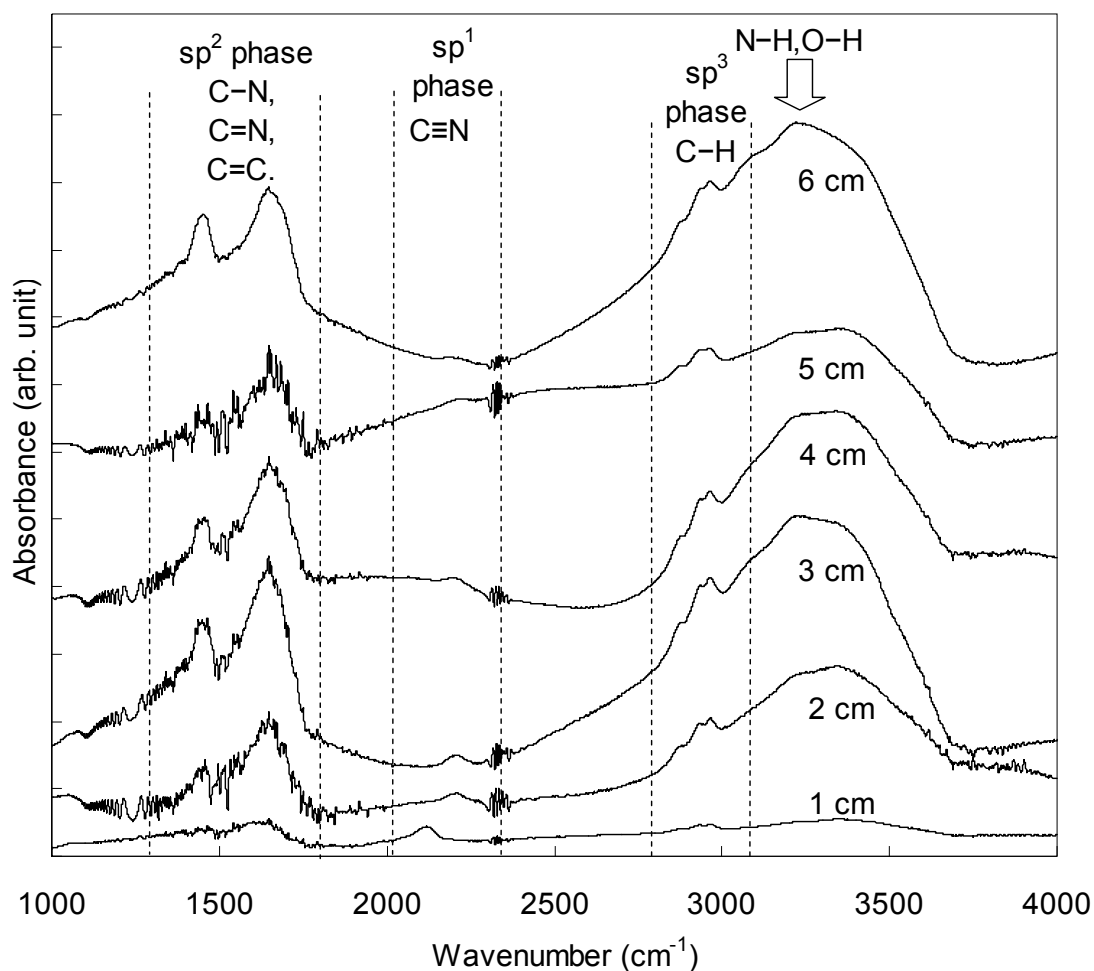
Figure 4.10: Variation in FTIR absorbance spectra for films deposited as a function of electrode distance in the range of 1000-4000 cm^{-1}.

Among these, a remarkable change is seen in the 1800–2200 cm^{-1} region, as shown in Figure 4.12, which is associated to the changes seen in the C≡N groups. According to the work of Mutsukura and Akita (Mutsukura and Akita 1999a), the broad band in this region can be decomposed into five overlapping bands associated with both nitrile (−C≡N) and isonitrile (−N≡C) structures. The peak positions of these bands depend strongly on the types of component bonded to these structures.
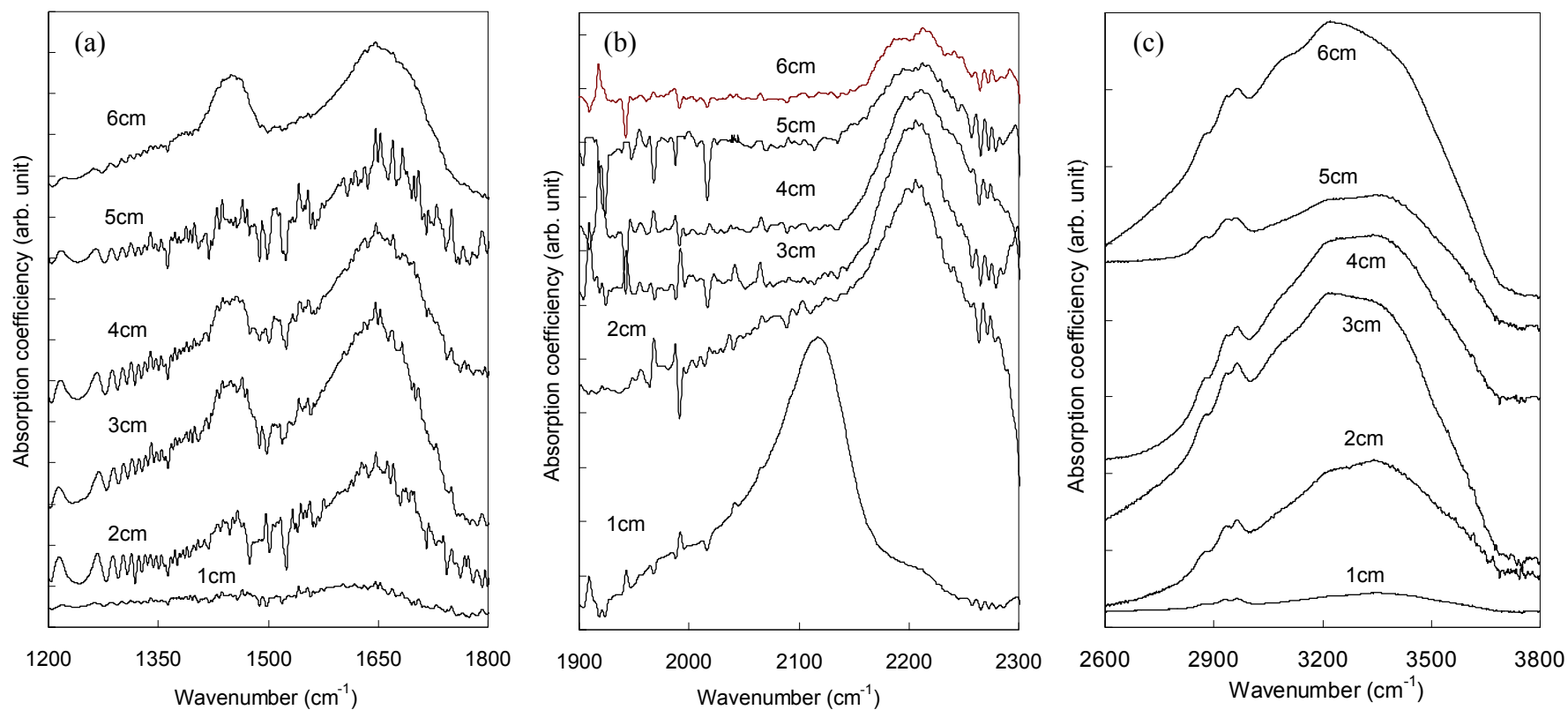
Figure 4.11: Variation in FTIR absorbance spectra for films deposited as a function of electrode distance

in the range of (a) sp^2, (b) sp^1 and (c) sp^3 phases.

These potential components includes the isolated and/or fused aromatic rings bonded either to isonitrile ($-$N$\equiv$C) at 2105 cm^{-1} or nitrile ($-$C$\equiv$N) at 2215 cm^{-1} and hydrocarbon molecules which includes C$_2$H$_5$ at 2160 cm^{-1} and CH$_3$ at 2190 cm^{-1} bonded to isonitrile ($-$N$\equiv$C) and the hydrocarbon groups (CH$_3$, C$_2$H$_5$, etc.) bonded to nitrile ($-$C$\equiv$N) located as a single peak at 2245 cm^{-1}.
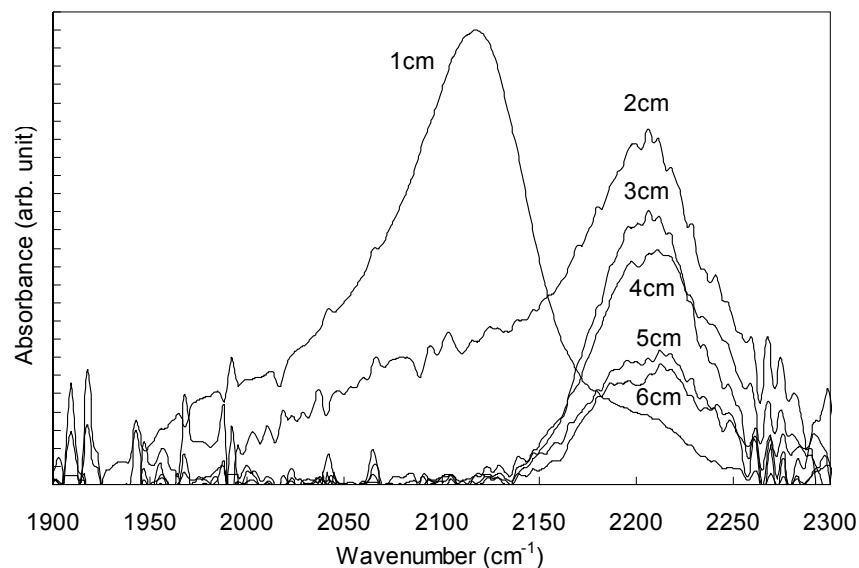
Figure 4.12: Variation in FTIR absorbance spectra for films deposited as a function of electrode distance in the range of 1900-2300 cm^{-1} for the C$\equiv$N region.

Using standard Gaussian fitting methods, the deconvolution of the spectra is obtained in this region and is shown in Figure 4.13. The band for the spectra of the films obtained at D$_E$ from 6-3 cm could be fitted to a single peak centered at 2215 cm^{-1} which is assigned to the bands of isolated and/or fused aromatic rings bonded to nitrile ($-$C$\equiv$N). With further decrease in D$_E$, a progressive broadening of these bands occurs and a significant shift in the maximum peak position to 2115 cm^{-1} is seen which is assigned to that of the isolated and/or fused aromatic rings bonded to isonitrile ($-$N$\equiv$C$-$).
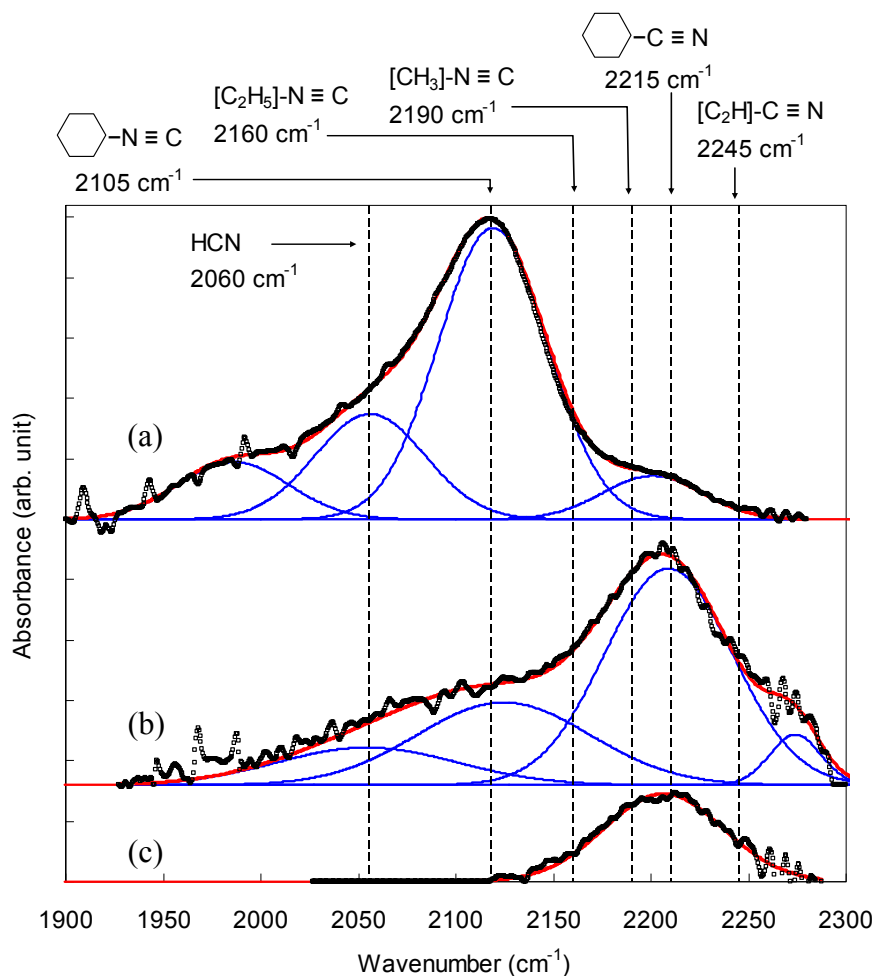
Figure 4.13: Gaussian fitting profiles for the FTIR spectra in the region of 1900-2300 cm^{-1} for the electrode distance of (a) 1cm, (b) 2cm and (c) 6cm. The blue line show the Gaussian fitting for the spectra (black points) and the red line shows the overall fitting curve.

Through these results, it is seen that one of the main differences in the bonding of the polymeric and nanostructured films is in the content and preferences in the nitrile or isonitrile bonds. The isonitrile tends to form rigid, linear and continuous non-terminating bonds (Muhl and Méndez 1999), which may imply the formation of long ordered networks in the material. In contrast, the nitriles are termination bonds which would lead to a shorter ordering range in the polymeric films. This indicates a significant change in the structure of the material and also a preferential requirement in the bonds to form either one of these structures.

The nitrile bonds formation results in the preferential formation of polymeric films while the isonitrile bonding results in the growth of nanostructured films. For the isonitrile bonds, preferential bonding of the ring through the N atom rather than C, and the additional connecting bond for N, suggests the presence of partial charge formed within the nanostructure strands. This means, the nitrogen atom will have a positive charge while C will be negatively charged [$-N^+\equiv C^-$]. Thus the resulting carbon network would have a partial charge imposed on it by the presence of this bond. From Figure 4.13 the absorbance intensity of this peak increases with the formation of the nanostructures both for D_E of 2 and 1 cm. Moreover as the structure progresses from the films grown at D_E of 2 to 1 cm, this peak becomes the preferential bond arrangement in the film which implies an increase in the contents of the charged [$-N^+\equiv C^-$] bonds. Furthermore, since the rf plasma is generating an electric field in a direction perpendicular to the substrate surface, it is believed that this electric field will induce aligned deposition of these polarized [$-N^+\equiv C^-$] bonds and contribute to the formation of the vertically-aligned CN$_x$:H nanostructures reported here.

4.3.5   Optical spectroscopy

Optical characterizations of the films were carried out on films deposited on quartz substrates. Though, as expected, the films deposited on these substrates are not identical to those deposited on c-Si with properties reported in the previous sections, the films do show structures which closely resembles them. It should also be noted that both sets of films (on c-Si and quartz substrates) were deposited simultaneously during the same deposition cycle. The film deposited at D_E of 1 cm on the quartz substrate is shown in Figure 4.14. Part of the film was intentionally scratched to expose the film and

enable the identification and observation of cross-sectional images of these structures. The nanostructures also grew vertically aligned though they are neither as oriented nor well-defined as those deposited on c-Si.
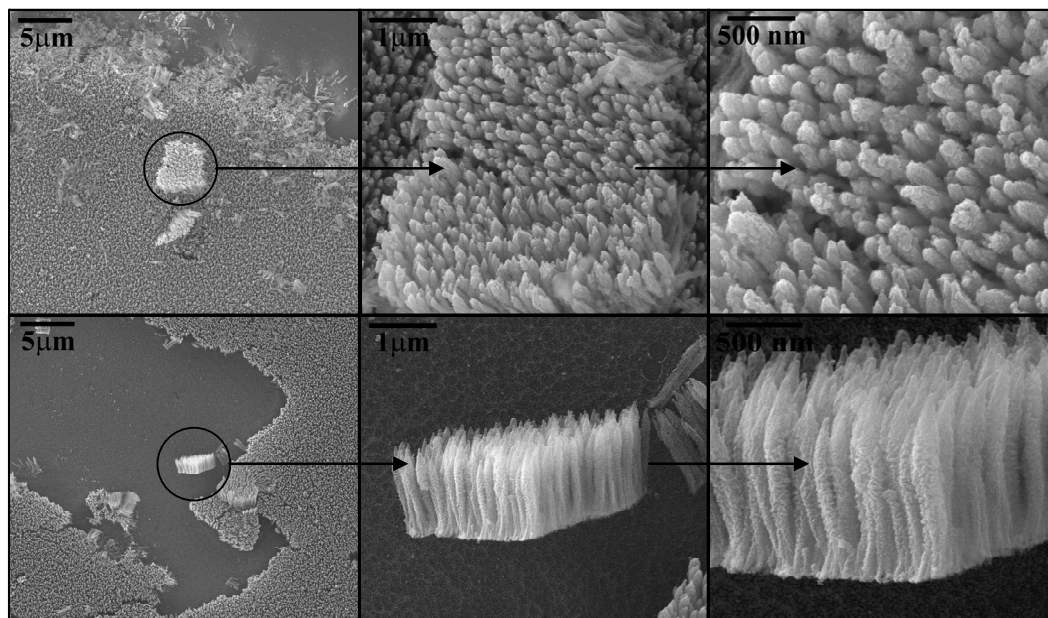
Figure 4.14: FESEM surface image of nanostructures grown on quartz substrate. Part of the film was intentionally scratched to expose the cross-sectional view of the nanostructures.

The variation of E_{04} as a function of D_E is shown in Figure 4.15. Interestingly, the trend for E_{04} reflects the variation in the growth rate which may actually be coincidental. However in general, the trend indicates that the E_{04} varies in a wide range and is highly dependent on deposition conditions and the structure of the films. E_{04} decreases in the D_E range of 6-3 cm, corresponding to the formation of the polymeric films. If one is to rely solely on the cluster model, this would mean that the decrease in E_{04} should reflect an increase in sp^2 graphitic cluster size. As discussed, the cluster model predicts that with the increase in the cluster size, the extended states size (and area) increases resulting in a decrease in the distance between the tail states and thus, the corresponding optical energy gap. However, the opposite is seen from Raman

scattering, where the graphitic cluster sizes decrease with the decrease in D_E. According to Robertson (Robertson 1997), when the sp^2 clusters are small, the decrease in band gap is due to the stronger influence of the distortion of rings or chains, and not on the cluster size since the distorted clusters have much smaller band gaps. This is supported by the Raman result which shows an increase in non six-fold rings in the sp^2-cluster together with a larger degree of bond angle or bond length disorder in the film. These distortions may widen the tail states or increase the defect states in the films causing the decrease in E_{04}.
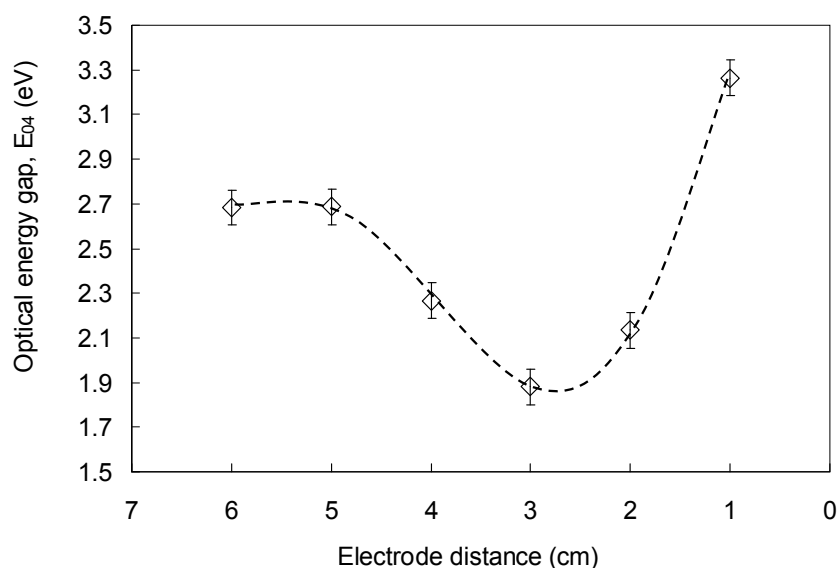
Figure 4.15: Variation in optical energy gap for films deposited as a function of electrode distance. The line is drawn as guide for the eye.

These effects are further reinforced by the increase in nitrogen content in the CN$_x$:H film (as shown in AES results). The sp^2-type incorporation of nitrogen would generate a significant amount of non six-fold atomic structures in CN$_x$ films (Andújar et al. 2001; Durand-Drouhin et al. 2001; Fanchini et al. ; Fitzgerald et al. 2001; Kola et al. 1995; Kovács et al. 2008; Lee et al. 2005; Li et al. 2002; Liu et al. 2001b; Neuhaeuser et al. 2000). This increases the disorder and causes further extension of tail states into the gap (Yoon et al. 1999). Furthermore, as seen from the FTIR results, contribution of sp^1-

type coordination increases with the decrease in D$_E$. This is verified from the increase in nitrile [–C≡N] bonds in the wavenumber range of 1800–2200 cm^{-1}. According to Fanchini et al (Fanchini et al. 2002a), the sp^1-hybridized C atoms from these C≡N bonds would yield specific lone-pair electronic states. The lone pairs, belonging to the nitrogen atoms, strongly influence the optical properties of CN$_x$ films. They have discussed the modification of the π-π* transition due to the interactions with these nitrogen lone pairs, and their correlation with optical modelling. It is said that for floppy (polymeric and amorphous) materials, the lone pair will interact with the molecular π orbital formed by neighbouring clustered C and/or N atoms. The energy of the lone pairs and these π states could be quite close, thus favouring "orbital mixing" effects (Fanchini et al. 2002a). This in turn would result in the formation of a single "lone pair- π" band of localized states which would result in the appearance of a broadening of the π band of the film due to a broadening of the density of states.

In contrast to the E$_{04}$ variation for the polymeric films, E$_{04}$ increases drastically as D$_E$ is further reduced from 2 to 1 cm, corresponding to the formation of the nanostructured films. However the validity of the increase in E$_{04}$ is doubtful particularly for D$_E$ of 1cm which forms the vertically aligned nanostructures. This arises from the considerable difference in its transmission and reflectance spectra compared to the rest of the films. These spectra, as indicated in Figure 3.9 (a) and (b) of Chapter 3, shows significantly lower intensities which may be the result of a large degree of dispersion and scattering of the incident beam (of the UV Vis-NIR spectrometer) on the surface of the film and walls of the nanostructures. Similar phenomenon could also occur in the nanostructured film for D$_E$ of 2 cm. Thus the current measurement method employed may not be appropriate for the nanostructured films and the increase in E$_{04}$ may not be due to the same reasons as that of the polymeric films.

4.3.6   Photoluminescence spectroscopy

The variation in PL spectra for CN$_x$:H as a function of D$_E$ is shown in Figure 4.16.
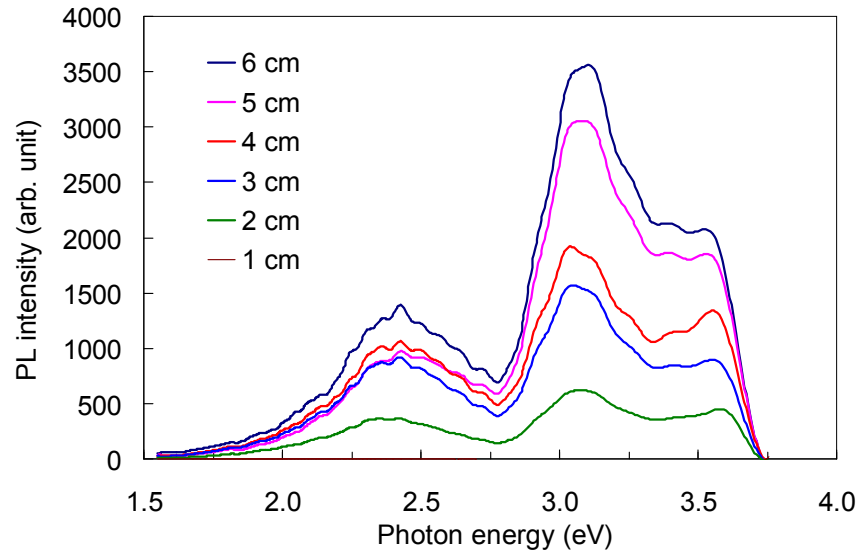
Figure 4.16: Variation in optical energy gap for films deposited as a function of electrode distance. The line is drawn as guide for the eye.

The PL spectra for D$_E$ of 1 cm could not be observed since it may be lower that the detection capability of the instrument. From the spectra themselves, there are roughly three main peaks that could be identified. These are located at approximately (2.42 ± 0.02), (3.05 ± 0.01) and (3.55 ± 0.02) eV, and are flanked by shoulder peaks at approximately (2.94 ± 0.01), (3.12 ± 0.01), (3.25 ± 0.01) and (3.42 ± 0.01) eV. This differs from other reports of CN$_x$ films (Daigo and Mutsukura 2004; Fanchini et al. 2003; Mutsukura and Akita 2000; Mutsukura 2001; Zhang et al. 1999b) which observed only a single broad peak centered between $1.80 - 2.40$ eV. There are some exceptions, one of which is the work done by Panwar et al (Panwar et al. 2006) which shows multiple peaks within a broad spectrum range of approximately 2.30-3.80 eV. However the assignment and the origin of the recombination centers of these peaks were not

clearly mentioned. For this work, the broad peak which is centered at 2.42 eV coincides with the single broad peak commonly found for CN$_x$ films. This peak is normally attributed to the π-π* transition within the sp^2 clusters. For most published works this peak is the dominant peak in the PL spectra which shows the role of the sp^2 clustering. However in this study it is overshadowed by a more significant stronger peak which is centered at around 3.05 eV. At this present time this peak (and the surrounding shoulder peaks) could not be identified with any certainty, though Zhang et al (Zhang et al. 1999b) has assigned a peak in the blue range of 460 nm (2.64 eV) being lower that the main peak at 540 nm, as arising from luminescence centers related to nitrogen bonding. On the other hand, the peak at 3.55 eV could be attributed to the σ-σ* transition in the Si (substrate) backbone (Zhang et al. 1999b).

For further analysis, these spectra were deconvoluted into five to six individual peaks using Gaussian fittings. These fittings are shown in Figure 4.17 and are made up of photon energy peaks at approximately (2.45 ± 0.05), (3.05 ± 0.06), (3.27 ± 0.06), (3.46 ± 0.05) and (3.60 ± 0.07) eV. The peak positions remain almost the same for each peak at different D_E. The significant difference is instead seen in the integrated intensities of these peaks. The variations in the peak intensities are shown in Figure 4.18.

The consistency in the peak position may indicate that the recombination centers for the films of each D_E may be the same resulting in the emission of a photon of similar energies. The difference instead is seen in the peak intensities which generally decrease with the decrease in D_E. Additionally for the polymeric films deposited at D_E of 3-6 cm, the intensities decreases with the decrease in E_{04}, in line with the variation usually attained for this material (Daigo and Mutsukura 2004; Robertson 2003).
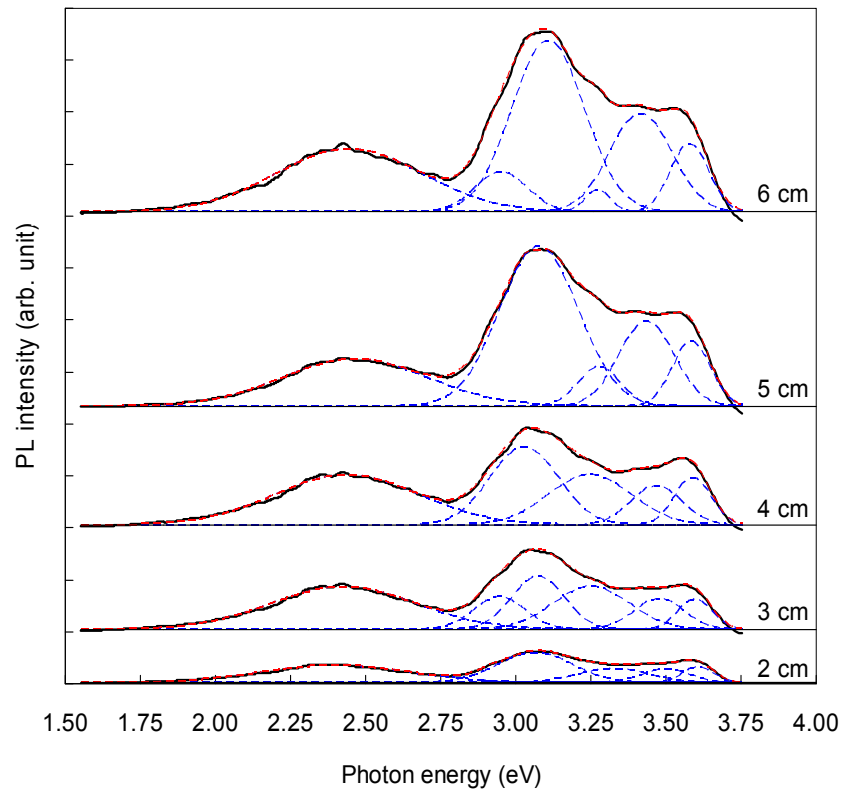
Figure 4.17: Gaussian fitting profiles for the PL spectra for D$_E$ of 6 to 2 cm. for the electrode distance of (a) 1cm, (b) 2cm and (c) 6cm. The blue line show the Gaussian fitting for the spectra (black points) and the red line shows the overall fitting curve.
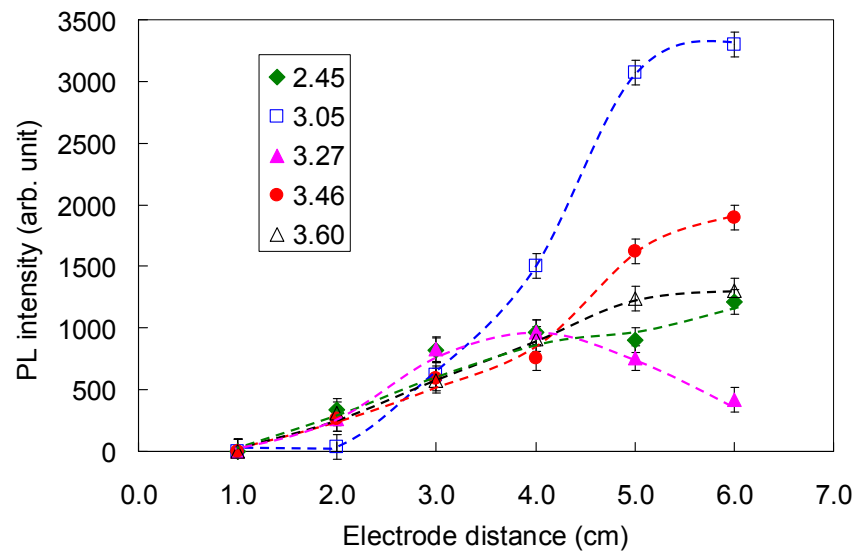
Figure 4.18: Variation in integrated PL intensities as a function of electrode distance. The line is drawn as guide for the eye.

It could be deduced from these results that the decrease in the PL intensities is attributed to an increase in defect states in the films. As seen from Raman, the reduction in D_E causes a decrease in number and/or size of the sp^2 clusters in the films and also a larger degree of bond angle and/or bond disorder. These changes may lead to a higher degree of disorder in the films whose contribution or effect on the PL properties is stronger than the positive contribution of the nitrogen. It is also seen from FTIR that although the incorporation of nitrogen increases the formation of C≡N, the changes in preferential bonding of nitrile to isonitrile with the decrease in D_E may also lead to the increase of unbonded lone-pairs which contributes to the defect sites causing a significant decrease in the PL intensities for the nanostructured films.

It should be noted that films deposited at higher D_E particularly at 6 cm show the highest PL intensities. It was shown from Raman and FTIR results that the properties of this film include the predominantly graphene-like clustering of the sp^2 sites and the formation of nitrile bonds which could contribute to the lone-pairs/π states. Indeed these two properties would form radiative recombination sites and thus increase the PL characteristics of the film.

4.4 Summary

Polymeric and nanostructured CN$_x$:H films were successfully produced using a simple home-built rf PECVD employing a parallel-plate electrode configuration. These two significantly different carbon nitride structures were produced at similar deposition conditions except for the difference of the electrode distance. This was presented in the first part of this result section, where a transformation from polymeric p-CN$_x$:H, to

nanostructured ns-CN$_x$:H films was induced though a simple manipulation of the electrode distance, D$_E$. The p-CN$_x$:H films were obtained within a separation range of D$_E$ of 6 to 3 cm, while ns-CN$_x$:H films were produced at 2 and 1 cm.

Upon further characterization and observations, two significant findings were put forward. The first is for the p-CN$_x$:H films where their PL emission was found to consist of a wide spectral range made up of a broad peak centered at 2.42 eV (512 nm) which is usually ascribed as the "green" emission and a strong peak centered at 3.05 eV ($\sim$ 407 nm) which is ascribed as "blue" emission. This differs from the normal single broad peak centered at approximately 540 nm found in most literature. The PL spectrum appears unique in which the peak positions do not vary much with D$_E$ and their intensities are highest for higher D$_E$ (6 and 5 cm). The results suggest that p-CN$_x$:H films with a larger or higher number of graphitic-like sp^2 clustering would exhibit higher PL emission.

The second finding is in the formation of the ns-CN$_x$:H films at lower D$_E$. The vertically aligned ns-CN$_x$:H films deposited at a D$_E$ of 1 cm is of particular interest since these structures could be obtained at low deposition temperatures (100-220 °C) without the assistance of metal catalysis and/or templates. To the best of the author's knowledge, no report of such findings has been published by other researchers. These results propose a very simple way to obtain ns-CN$_x$:H. Ion bombardment was seen to play a part in the formation of these structures. Apart from this, nitrogen incorporation is crucial in the formation of the ns-CN$_x$:H. Indeed without N$_2$ dilution the nanostructures were not produced and these were obtained at higher N incorporation than the p-CN$_x$:H films. There was found be to a relationship between the incorporation, structural and chemical bonding properties in the films. While the p-CN$_x$:H films

contain graphene-like sp^2 clusters, the nanostructures contain graphitic sp^2 clusters that are smaller and/or fewer in number. However, these clusters are of great significance in the formation of the ns-CN$_x$:H.

These two findings were used as the basis of the studies on the polymeric and nanostructured thin films in the following chapters.